Capillary Forces between Colloidal Particles Confined in a Liquid Film: The Finite-Meniscus Problem

ARTICLE *in* LANGMUIR · SEPTEMBER 2001

Impact Factor: 4.46 · DOI: 10.1021/la0107300

3 AUTHORS:

Krassimir Danov
Sofia University "St. Kliment Ohridski"
154 PUBLICATIONS **3,305** CITATIONS
SEE PROFILE

Bernard Pouligny
Centre de Recherche Paul Pascal
87 PUBLICATIONS **1,559** CITATIONS
SEE PROFILE

Peter Kralchevsky
Sofia University "St. Kliment Ohridski"
155 PUBLICATIONS **4,523** CITATIONS
SEE PROFILE

Capillary Forces between Colloidal Particles Confined in a Liquid Film: The Finite-Meniscus Problem

Krassimir D. Danov,[†] Bernard Pouligny,[‡] and Peter A. Kralchevsky*,[†]

Laboratory of Chemical Physics Engineering,[§] Faculty of Chemistry, University of Sofia, 1 J. Bourchier Avenue, Sofia 1164, Bulgaria, and Centre de recherche Paul-Pascal/CNRS, Avenue Schweitzer, Pessac 33600, France

Received May 16, 2001. In Final Form: July 23, 2001

We consider a system made of two spherical particles confined between two fluid interfaces. The concept is illustrated in experiments with polystyrene micrometer-sized particles located between the two membranes of a bilamellar giant lipid vesicle. The particles locally separate the membranes and form a "Plateau border", which is filled with water. Experiments based on optical manipulation and dynamometry readily show that the particles attract each other. The interaction force is long-ranged (several particle radii) and goes through a maximum (about a piconewton) at finite particle separation. We propose a theory of the interaction, based on the linearized Laplace equation for the meniscus profile. The theory predicts that the meniscus around an isolated particle is *finite*, that is, bounded by a peripheral contact line, outside of which the film surfaces are equidistant. When two particles come near each other, their menisci overlap and fuse to form a unique meniscus with a new peripheral line. This is the source of the capillary interaction. The computation yields a characteristic nonmonotonic force-versus-distance profile, as experimentally observed with the latex particles. The computed profile quantitatively fits to the experimental data, with a single adjustable parameter, the bilayer tension. Other features of the interaction (hysteresis, dependence on particle size) are discussed. We find that the capillary attraction in general is strong enough to cause aggregation of the confined colloidal particles.

1. Introduction

1.1. Types of Capillary Forces. Colloidal particles attached to a fluid interface or confined in a liquid film as a rule produce interfacial deformations (menisci). The overlap of the menisci formed around two separate particles gives rise to a lateral capillary force between them, which is usually attractive; for a detailed review, see refs 1 and 2. Depending on the nature of the interfacial deformations, two types of lateral capillary forces can be distinguished:

(i) In the case of *flotation* forces, the meniscus is due to the weight (incl. buoyancy force) of floating particles.[3−10] This force causes two-dimensional aggregation of floating particles;[9,10] its magnitude is proportional to R_p^6 (R_p = particle radius). For that reason, the flotation capillary force strongly decreases with the decrease of R_p and becomes immaterial for R_p smaller than ca. 5 μm.[1,2,9,11]

(ii) The other type of capillary force, the *immersion* force, appears between particles that are confined in a liquid film with one or two deformable surfaces (Figure 1a,b).[12] In this case, the deformation is related to the wetting properties of the particle surfaces (contact angles, edges) rather than to gravity. The immersion force can be significant between particles whose radii are larger than a few nanometers.[1,2,9,11] It has been found to promote the growth of two-dimensional crystals from colloid particles,[13−16] viruses, and globular proteins.[17−22] Such two-dimensional crystals have found various applications: for nanolithography,[23] for microcontact printing,[24] as nanostructured materials in photoelectrochemical cells,[25] for photocatalytic films,[26] as photo- and electroluminescent semiconductor materials,[27] as samples for electron mi-

[†] University of Sofia.

[‡] Centre de recherche Paul-Pascal/CNRS.

[§] Formerly Laboratory of Thermodynamics and Physicochemical Hydrodynamics.

(1) Kralchevsky, P. A.; Nagayama, K. *Adv. Colloid Interface Sci.* **2000**, *85*, 145.
(2) Kralchevsky, P. A.; Nagayama, K. *Particles at Fluid Interfaces and Membranes*; Elsevier: Amsterdam, 2001.
(3) Nicolson, M. M. *Proc. Cambridge Philos. Soc.* **1949**, *45*, 288.
(4) Gifford, W. A.; Scriven, L. E. *Chem. Eng. Sci.* **1971**, *26*, 287.
(5) Fortes, M. A. *Can. J. Chem.* **1982**, *60*, 2889.
(6) Chan, D. Y. C.; Henry, J. D.; White, L. R. *J. Colloid Interface Sci.* **1981**, *79*, 410.
(7) Somasundaran, P.; Varbanov, R.; Tchaliovska, S. *Colloids Surf.* **1992**, *64*, 35.
(8) Israelachvili, J. N. *Intermolecular and Surface Forces*; Academic Press: London, 1992.
(9) Paunov, V. N.; Kralchevsky, P. A.; Denkov, N. D.; Nagayama, K. *J. Colloid Interface Sci.* **1993**, *157*, 100.
(10) Allain, C.; Cloitre, M. *J. Colloid Interface Sci.* **1993**, *157*, 261, 269.
(11) Kralchevsky, P. A.; Nagayama, K. *Langmuir* **1994**, *10*, 23.
(12) Kralchevsky, P. A.; Paunov, V. N.; Ivanov, I. B.; Nagayama, K. *J. Colloid Interface Sci.* **1992**, *151*, 79.
(13) Denkov, N. D.; Velev, O. D.; Kralchevsky, P. A.; Ivanov, I. B.; Nagayama, K.; Yoshimura, H. *Langmuir* **1992**, *8*, 3183.
(14) Dimitrov, A. S.; Dushkin, C. D.; Yoshimura, H.; Nagayama, K. *Langmuir* **1994**, *10*, 432.
(15) Sasaki, M.; Hane, K. *J. Appl. Phys.* **1996**, *80*, 5427.
(16) Du, H.; Chen, P.; Liu, F.; Meng, F.-D.; Li, T.-J.; Tang, X.-Y. *Mater. Chem. Phys.* **1997**, *51*, 277.
(17) Price, W. C.; Williams, R. C.; Wyckoff, R. W. G. *Science* **1945**, *102*, 277.
(18) Cosslett, V. E.; Markham, R. *Nature* **1948**, *161*, 250.
(19) Horne, R. W.; Pasquali-Ronchetti, I. *J. Ultrastruct. Res.* **1974**, *47*, 361.
(20) Harris, J. R. *Micron Microsc. Acta* **1991**, *22*, 341.
(21) Yamaki, M.; Higo, J.; Nagayama, K. *Langmuir* **1995**, *11*, 2975.
(22) Nagayama, K. *Colloids Surf., A* **1996**, *109*, 363.
(23) Burmeister, F.; Schäfle, C.; Keilhofer, B.; Bechinger, C.; Boneberg, J.; Leiderer, P. *Adv. Mater.* **1998**, *10*, 495.
(24) Xia, Y.; Tien, J.; Qin, D.; Whitesides, G. M. *Langmuir* **1996**, *12*, 4033.
(25) Lindstrom, H.; Rensmo, H.; Sodergren, S.; Solbrand, A.; Lindquist, S. E. *J. Phys. Chem.* **1996**, *100*, 3084.
(26) Matsushita, S.; Miwa, T.; Fujishima, A. *Langmuir* **1997**, *13*, 2582.
(27) Murray, C. B.; Kagan, C. R.; Bawendi, M. G. *Science* **1995**, *270*, 1335.

10.1021/la0107300 CCC: $20.00
Published on Web 09/22/2001

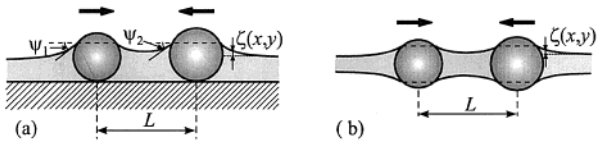

Figure 1. The capillary "immersion" force is due to the overlap of the menisci formed in a vicinity of colloidal particles confined in liquid films. (a) Two particles in a wetting film on a solid substrate. (b) Two particles in a free film; $z = \zeta(x,y)$ describes the meniscus shape (deviation from planarity).

croscopy of proteins and viruses,[28] as immunosensors,[29] and so forth.

1.2. Infinite versus Finite Extent of the Meniscus. The theoretical description of the lateral capillary forces is based on the Laplace equation,[30] which determines the shape of the liquid meniscus $z = \zeta(x,y)$. In general, it is a second-order nonlinear partial differential equation:[31]

$$\sigma\nabla_{II}\cdot\left[\frac{\nabla_{II}\zeta}{(1+|\nabla_{II}\zeta|^2)^{1/2}}\right] = P_c \qquad (1.1)$$

where σ is the surface tension and P_c is the capillary pressure (the pressure difference across the meniscus).

$$\nabla_{II} \equiv \mathbf{e}_x\frac{\partial}{\partial x} + \mathbf{e}_y\frac{\partial}{\partial y} \qquad (1.2)$$

is the two-dimensional gradient operator in the xy-plane. When the particles only slightly deform the interfaces, that is, when the slopes are small ($|\nabla_{II}\zeta|^2 \ll 1$) and the perturbations are small compared with the nondisturbed film thickness ($\zeta/h_0 \ll 1$), the Laplace equation (eq 1.1) simplifies into the linear form:[1,2,12]

$$\nabla_{II}{}^2\zeta = q^2\zeta \qquad q^2 \equiv \frac{\Delta\rho g}{\sigma} + \frac{-\Pi'}{\sigma} \qquad (1.3)$$

where q^{-1} is the characteristic decay length of the interfacial deformation and of the lateral capillary force; $\Delta\rho$ is the difference between the mass densities of the two neighboring fluid phases; g is the acceleration due to gravity; $\Pi' = (\partial\Pi/\partial h)_{h=h_0}$ is the derivative of the disjoining pressure Π with respect to the film thickness h. In *thick* films ($\Pi' \to 0$), the gravity keeps the fluid interface planar far from the particle; in this case, $q^{-1} = (\Delta\rho\, g/\sigma)^{-1/2}$ is the usual capillary length. In contrast, in *thin* films ($|\Pi'| \gg \Delta\rho\, g$) the repulsive disjoining pressure keeps the liquid film plane-parallel; then the characteristic decay length $q^{-1} \approx (-\Pi'/\sigma)^{-1/2}$ is determined by the disjoining-pressure effect (the surface forces).[11,12]

Using cylindrical coordinates (r,φ) in eq 1.3, one can determine the shape of the meniscus around a single particle in the form

$$\zeta(r) = A\, K_0(qr) \qquad (1.4)$$

where K_0 is the modified Bessel function of the second kind and zeroth order and A is a constant of integration. The corresponding meniscus is exponentially decaying at infinity.[32] For the sake of brevity, we will call such a meniscus "infinite". Further, one can apply the superposition approximation, that is, assume that the interfacial deformation caused by two particles (Figure 1) is equal to the sum of the deformations caused by the separate particles in isolation.[3,6] Then, in view of eq 1.4, the energy of lateral capillary interaction between the two particles can be expressed in the form[1,2,6,11]

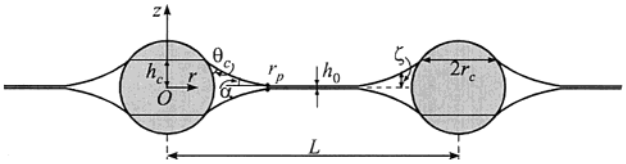

Figure 2. Two colloidal spheres entrapped in a free liquid film of thickness h_0, which is much smaller than the particle diameter. Plateau borders of outer radius r_p and peripheral contact angle α are formed around each sphere; θ_c is a solid−liquid−fluid contact angle.

$$\Delta W \approx -2\pi\sigma Q_1 Q_2 K_0(qL) \qquad (1.5)$$

where L denotes the distance between the two particles, $Q_i \equiv r_i \sin\psi_i$ $(i = 1,2)$ are the so-called "capillary charges", and r_i and ψ_i are the radius of the contact line and the slope angle at the contact line of the respective particle (see Figure 1 for the notation). ΔW represents a variation in the gravitational energy or in the energy of wetting for flotation or immersion forces, respectively. For long distances, $\Delta W \propto (qL)^{-1/2}\exp(-qL)$.

Equation 1.3 is not valid for all physically possible cases. Indeed, the relationship $\zeta/h_0 \ll 1$ corresponds to comparable magnitudes of the particle diameter and film thickness. However, it is possible that the particle size be much greater than the film thickness, $\zeta/h_0 \gg 1$, see Figure 2. Then, instead of eq 1.3, the meniscus profile obeys the equation

$$\sigma\nabla_{II}{}^2\zeta = P_c = \text{const} \qquad (\zeta/h_0 \gg 1,\ |\nabla_{II}\zeta|^2 \ll 1) \quad (1.6)$$

Equation 1.6 follows from eq 1.1, where in the denominator $|\nabla_{II}\zeta|^2$ is neglected in comparison to 1; as before, P_c is the pressure jump across the meniscus; P_c is constant if the effect of the gravitational hydrostatic pressure is negligible. The general solution of eq 1.6 for a meniscus of rotational symmetry reads[33]

$$\zeta(r) = A + B\ln r + (P_c/4\sigma)r^2 \qquad (1.7)$$

where A and B are constants of integration. The comparison of eqs 1.4 and 1.7 shows that, unlike eq 1.3, eq 1.6 has no axisymmetric solutions which are finite at infinity ($r \to \infty$). The latter fact implies that the meniscus around a particle must end at a *peripheral contact line* (of radius r_p), out of which the film is plane-parallel ($\zeta \equiv 0$), see Figure 2; we will call such a meniscus "finite". In this case, the overlap of the menisci, and the interaction between the particles, begins when they come at a distance $L < 2r_p$ from each other. This type of interaction is obviously different from that described by eq 1.5.

In our experiments, the largest meniscus slope is 8.5° (see section 3.2 below) which makes possible to use the linearized eq 1.6. In the general case, one has to use the nonlinear eq 1.1.

(28) Jap, B. K.; Zulauf, M.; Scheybani, T.; Hefti, A.; Baumeister, W.; Aebi, U.; Engel, A. *Ultramicroscopy* **1992**, *46*, 45.
(29) De Rossi, D.; Ahluwalia, A.; Mulè, M. *IEEE Eng. Med. Biol.* **1994**, *13*, 103.
(30) Laplace, P. S. *Traité de mécanique céleste*, suppléments au Livre X; 1805.
(31) Finn, R. *Equilibrium Capillary Surfaces*; Springer-Verlag: New York, 1986.
(32) Princen, H. M. The Equilibrium Shape of Interfaces, Drops, and Bubbles. In *Surface and Colloid Science*; Matijevič, E., Ed.; Wiley: New York, 1969; Vol. 2, p 1.
(33) Korn, G. A.; Korn, T. M. *Mathematical Handbook*; McGraw-Hill: New York, 1968.

1.3. Subject and Plan of the Paper. The problem of the capillary immersion force has not yet been addressed theoretically for menisci of *finite* extent, whose shape is governed by eq 1.6. This problem deserves to be investigated insofar as the aforementioned situation, that is, inclusions much larger than the film thickness, can be experimentally realized. For example, Velikov et al.[34] observed a strong attraction between latex particles of diameter $2R_p \approx 7\ \mu$m entrapped in a foam film whose thickness was at least 100 times smaller. Similar attraction has been observed by Sur and Pak,[35] who investigated the meniscus-mediated interactions between a particle, sandwiched in a foam film, and the surrounding Plateau border.

In section 2 below, we describe analogous observations with micrometer-sized latex spheres encapsulated within the bilamellar membrane of a giant lipid vesicle. These experiments, based on optical manipulation and dynamometry (optical tweezers), neatly reveal the film deformation caused by the particles and the related attraction between them. Experimental data are analyzed in section 3: basic characteristics of the meniscus are deduced from photographs of the vesicle−particle system, and the experimental capillary force profile is found from the analysis of a two-particle trajectory. The theory is worked out in section 4: mathematical principles are set out to calculate the shape of the two-particle meniscus and the related capillary immersion force and energy. Comparing the theory and the experimental data is the matter of section 5. As we will see, the experimental data for the trajectory of a couple of latex particles can be quantitatively accounted for by the theory. Section 6 is a discussion on some characteristics of capillary immersion forces in the case of *finite* menisci. The main results of the paper are summarized in section 7. Appendix A contains a tentative explanation for the mechanism of particle encapsulation in the vesicle bilamellar membrane. Appendix B gives the main steps of the numerical procedure used to compute the force and energy profiles.

2. Experiments with Latex Particles Attached to Lipid Vesicles

2.1. Giant Lipid Vesicles. Phospholipids in water self-assemble into bilayers about 4 nm in thickness. Different preparation procedures allow production of vesicles, whose membranes are constituted of one or a few such lipid bilayers.[36] In our experiments, we used so-called "giant vesicles", grown by electroformation.[37] The method produces a cluster of vesicles on the surface of a platinum electrode. The vesicles at the outer boundary of the cluster are approximately spherical, with diameters in the 10−100 μm range. On their "rear" sides (toward the electrode), they are connected to neighboring vesicles by a few contact points, sometimes by a small adhesion area. Their outer sides are free of contacts. Electroformation is a nice method to produce unilamellar giant vesicles. Nevertheless, multilamellar specimens can be found in the cluster, in proportions that subtly depend on the used lipid and on the parameters of the procedure.

In our experiments, we used SOPC, that is, 1-stearoyl-2-oleoyl-*sn*-glycero-3-phophocholine, which is a synthetic, *zwitterionic* double-chained lipid. In some experiments, we used also cationic vesicles prepared from the mixture SOPC/Sph+, 80:20 mol/mol, where Sph+ stands for D-Erythro-Sphingosine (brain), a *cationic* single-chained amino-alcohol. Both substances are products of Avanti Polar Lipids.

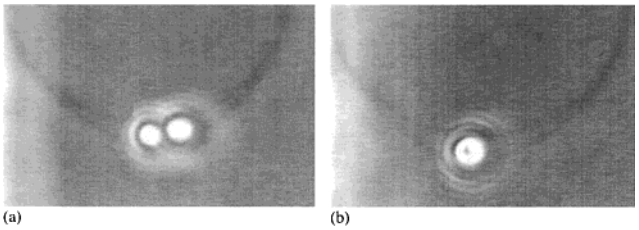

Figure 3. Photos of a couple of latex beads trapped between two detached lipid membranes composing a bilamellar spherical vesicle. Each photo is an equatorial cut of the vesicle. (a) The two beads are side by side in the same equatorial plane. (b) Section perpendicular to the line that goes through the centers of the beads; the two beads are still present, but one is just on top of the other.

2.2. Latex Particle Attachment to a Vesicle. The experiment of interest here is one of many which were carried out[37,38] to study the interactions of polystyrene latex particles with the membranes of giant lipid vesicles. We use an optical trap[39] to manipulate single particles and bring them in contact with vesicles. It is generally observed that simple latex spheres (whose surfaces bear sulfate groups) spontaneously adhere to neutral (zwitterionic) lipid vesicles.[37] The membranes in the photographs below (Figure 3) were in fact positively charged (from the 80:20 SOPC/Sph+ mixture), but similar behaviors, in terms of particle encapsulation and capillary interactions, were observed with neutral vesicles.

When a particle gets in contact to a lipid membrane, different scenarios may happen, leading to a partial wetting of the particle surface by the lipids or to a complete encapsulation.[37,40] The photos in Figure 3 reveal that the vesicle was bilamellar. Each particle was incorporated between two lipid lamellae and pushed them apart, creating a water gap in between.[41] In this experiment, the particle diameter, $2R_p$, was about 4.3 μm, and the vesicle diameter, $2R_v$, was 39 μm. Below, we will use the term "Plateau border" for this narrow region filled with water, making analogy with the similar formations in foams. At the present stage, the dynamics of particle incorporation and membrane delamination is not completely understood (see Appendix A for a discussion), but this is not the important point here, inasmuch as we are interested only in the final configuration. Indeed, the experiment is a physical realization of the configuration sketched in Figure 2, that is, a film with two solid inclusions whose diameters, 4.3 μm, are considerably greater than the equilibrium film thickness (a few nanometers).

2.3. Interaction between Two Attached Particles. The optical setup can be operated in a double trap configuration[39] (two pairs of laser beams). This allowed us to catch each particle and to vary the interparticle separation. For instance, starting with the configuration of Figure 3a, that is, with both particles in the vesicle equatorial plane, we pulled them apart. When the particles were separated, we switched off the beams and noticed that the particles would move back toward contact, proving

(34) Velikov, K. P.; Durst, F.; Velev, O. D. *Langmuir* **1998**, *14*, 1148.
(35) Sur, J.; Pak, H. K. *J. Korean Phys. Soc.* **2001**, *38*, 582.
(36) Dimova, R.; Dietrich, C.; Pouligny, B. In *Giant Vesicles*; Luisi, P., Walde, P., Eds.; John Wiley & Sons: New York, 1999; p 222.
(37) Dietrich, C.; Angelova, M.; Pouligny, B. *J. Phys. II France* **1997**, *7*, 1651.
(38) Dimova, R.; Dietrich, C.; Hadjiisky, A.; Danov, K.; Pouligny, B. *Eur. Phys. J. B* **1999**, *12*, 589.
(39) Angelova, M. I.; Pouligny, B. *Pure Appl. Opt.* **1993**, *2*, 261.
(40) Pouligny, B.; Martinot-Lagarde, G.; Angelova, M. I. *Prog. Colloid Polym. Sci.* **1995**, *98*, 280.
(41) Danov, K. D.; Pouligny, B.; Angelova, M. I.; Kralchevsky, P. A. In *Studies in Surface Science and Catalysis*; Iwasawa, Y., Oyama, N., Kunieda, H., Eds.; Elsevier: Amsterdam, 2001; Vol. 132, p 519.

the existence of a long-range (micrometers) attraction. The observation could be repeated at will.

The maximum horizontal force which is produced by each optical trap on each particle is proportional to the laser power. For instance, a power equal to 4 mW results in a force of about 1 piconewton (pN).[42] We observed that this force was sufficient to separate the particles when these were in contact. However, this force allowed us to increase the particle separation (the surface-to-surface distance, s) only up to about 2 μm. Beyond this separation, the capillary attraction became so strong that the particles escaped from the optical traps and stuck together again. This observation shows that the capillary attraction increases when s increases (starting from 0). On the other hand, the interaction should vanish for very large separations. Clearly, the attraction reaches a maximum, F_{max}, for some intermediate distance $s = s^*$. The conclusion from the above observation is $F_{max} \geq 1$ pN and $s^* \geq 2$ μm.

As already mentioned, the observation was repeatable. Here, we want to make a distinction between this "repeatability", which is related to one and the same system, and "reproducing the experiment", in the sense of elaborating the same system from a new preparation and observing the capillary interaction again. In fact, we observed capillary attractions only sporadically among hundreds of different systems. The above-described system was an ideal realization, because it combined a bunch of desirable features: (i) the vesicle was bilamellar, (ii) the particles were spontaneously encapsulated between the lipid bilayers, (iii) the volume of encapsulated water was large enough to neatly separate the membranes and build large menisci around the particles, and (iv) the sizes of the particles were large enough for the geometry of the system (the meniscus shape) to be well observable by microscopy and small enough to avoid stress-induced lysis of the vesicle.[37] In electroformed vesicle clusters, conditions i−iii are not controlled by the experimentalist. For instance, it is hard to note a difference between uni- and bilamellar vesicles through microscope observation only. Besides, the way in which the particles insert themselves between the membranes is not known in principle. It depends at least on the vesicle tension, which is not known a priori. For these reasons, reproducing a system such as that studied in this paper, that is, with prescribed values of all the relevant parameters, is not directly feasible. However, it is possible to produce *similar systems*, with different values of the membrane tension and of the encapsulated volume, but this demands many attempts, with many vesicles (hundreds, as we told).

In the experiment reported in ref 43, we observed that the small particles (2 μm in diameter) would spontaneously form clusters and that these clusters would gain and lose particles all the time, within a few seconds. This suggests that the pair interaction potential of two particles at contact was on the order of kT. In addition, we observed capillary attraction between two large particles (diameter $2R_p = 15$ μm) in a few examples. The particles went in contact, but it was not possible to separate them with the optical trap, even with the laser pushed at maximum power. The corresponding radiation pressure force was about 20 pN per particle, and the work done on each particle by the optical trap was on the order of 2×10^{-9} erg. This corresponds to about 10^5 kT. The experiment indicates that the attraction energy of the particles at contact was definitely larger than this value. Apparently, the attraction strongly increases with the particle size.

2.4. Kinetics. We studied the motions of both particles on the vesicle, in various conditions. Essentially, the motion was driven by gravity and by the capillary interaction. Brownian motion was secondary. By optical manipulation, we first located a particle, say particle 1, near the bottom (south pole) of the vesicle and brought the other one, say particle 2, near the top (north pole) and then switched off the laser beams. Particle 1 hardly moved, while particle 2 started its descent down to the vesicle equator. When it was below the equator, particle 2 accelerated while particle 1 started moving up toward particle 2, until collision and attachment.

The analysis of the particle trajectories (see ref 38 for the detailed procedure) shows that the first part of the motion, that is, when particle 2 was above the equator, was a pure sedimentation. Otherwise stated, there was no trace of a capillary interaction when the angular separation (denoted θ in the following) between the particles was larger than 90°. From the particle trajectory in this regime, we deduced the value of the particle drag coefficient, B. Taking $B_0 = 6\pi\eta R_p$, the Stokes drag coefficient in bulk water, as a reference, we found $B = f_1 B_0$, with $f_1 \approx 2.1$. In other words, the particle attached to the vesicle felt a hydrodynamic friction which was more than twice that in bulk water.

The plot in Figure 4a is an example of a two-particle trajectory (θ versus time) when the initial separation is about 80°, that is, when the capillary attraction is operative. The discontinuity in the beginning of the experimental curve corresponds to the moment at which the optical trap was switched off and the two particles were allowed to move toward each other under the action of the attractive capillary immersion force. Clearly, the velocity goes through a maximum, corresponding to about 6 μm for the gap between the particles (see Figure 4b). This suggests that the capillary attraction is maximum before the particles get in contact, in concordance with the observation based on optical dynamometry.

3. Data Analysis

3.1. Two-Particle Trajectory and Force Balance Scheme. The second Newton's law for the particle motion reads

$$m R_v \ddot{\theta} = -[F_c(s,\sigma) - F_d(s)] \qquad \ddot{\theta} \equiv \frac{d^2\theta}{dt^2} \tag{3.1}$$

where m is the mass of the particle, R_v is the radius of the vesicle, and t is time. The distance between the two particles can be represented by θ, their angular separation (Figure 4a), or by $s = \theta R_v - 2R_p$, the width of the gap between them. The capillary force, F_c, depends on s and on the bilayer tension, σ. The computation of F_c is described in section 4.2. The hydrodynamic drag force, F_d, acting on each particle, can be expressed as

$$F_d = 6\pi\eta R_p v f_1 f_2 \qquad (v = R_v\dot{\theta}) \tag{3.2}$$

Here, η is the viscosity of the aqueous phase and v is the velocity of the particle. The Stokes term, $6\pi\eta R_p v$, is the drag force experienced by a particle moving in the bulk of the water phase; f_1, already defined in section 2.4, is a

(42) This concerns the particle and beam characteristics of our experiments. The precise result, 0.27 pN/mW, was obtained from the Generalized Lorenz−Mie theory; see: Martinot-Lagarde, G.; Pouligny, B.; Angelova, M. I.; Gréhan, G.; Gouesbet, G. *Pure Appl. Opt.* **1995**, *4*, 571 and references therein.

(43) Angelova, M. I.; Pouligny, B.; Martinot-Lagarde, G.; Grehan, G.; Goulesbet, G. *Prog. Colloid Polym. Sci.* **1994**, *97*, 293.

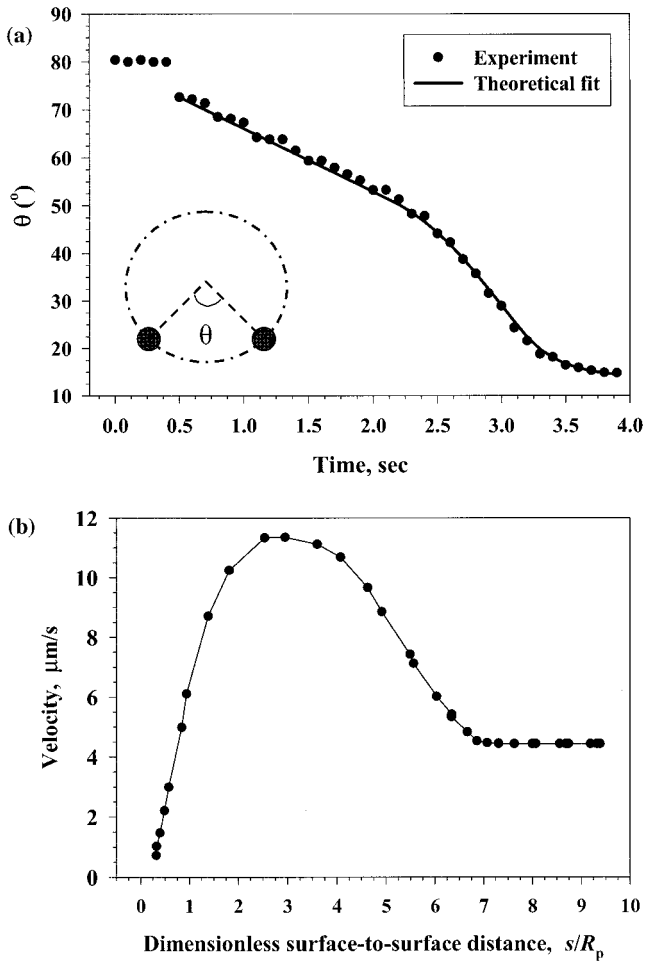

Figure 4. (a) Theoretical fit of the experimental particle trajectory $\theta(t)$; here, θ is central angle (angular distance) and t is time. (b) Plot of the particle velocity, v, vs the surface-to-surface distance, $s \equiv L - 2R_p$, scaled with the particle radius, R_p.

coefficient taking into account the excess hydrodynamic friction due to the fact that each *separate* particle is attached to the lipid vesicle.[44] As we explained, f_1 was experimentally measured and found to be ≈ 2.1. f_2 is a factor which accounts for the hydrodynamic interaction between the *two* approaching particles. To estimate the value of f_2, we utilize the formula of Stimson and Jeffrey,[45] which was derived for the case of two spherical particles approaching each other in a bulk viscous fluid:

$$f_2 = \sum_{n=1}^{\infty} n(n+1)\frac{\sinh\epsilon}{6\Delta_n}\left[\frac{\lambda_n}{\lambda_{n-1}}\exp(2\epsilon) + \frac{\lambda_n}{\lambda_{n+1}}\exp(-2\epsilon) + \frac{2}{\lambda_{n-1}\lambda_{n+1}}\exp(-2\lambda_n\epsilon) - 2\right] \quad (3.3)$$

where

$$\lambda_n \equiv (2n+1)/2 \quad (3.4)$$

$$\Delta_n \equiv \sinh(2\lambda_n\epsilon) - \lambda_n \sinh(2\epsilon) \quad (3.5)$$

$$\cosh\epsilon = 1 + \frac{s}{2R_p} \quad (3.6)$$

For long distances ($s \to \infty$), eq 3.3 gives $f_2 \to 1$ (no hydrodynamic interactions), as one might expect. In the other limit, $s \to 0$, eq 3.3 reduces to the known Taylor formula,[2,46] that is, $f_2 \propto 1/s$. Values of f_2, calculated for the range of variation of s in our experiments, are shown in Figure 5. (In the analysis of experimental data, s was taken as the length of the shortest arc of radius R_p between the two particles.) At short separations, f_2 rises up to 3.5 and tends to considerably decelerate the particle motion at short distances (small s).

Equation 3.3, originally derived for two particles in bulk liquid, is applied here for interactions between membrane-sandwiched particles. Unfortunately, for the time being there is no exact solution of the hydrodynamic problem for our compartmentalized system. Nevertheless, we expect that eq 3.3 could provide a good approximation owing to the following reasons:

(i) The viscosity of the lipid membranes is much larger than that of water (10 vs 0.01 P, see refs 38 and 47). Consequently, the hydrodynamic perturbations along the lipid membranes, caused by the particle motion, decay at much smaller distances from the particle surfaces than those in water. Therefore, the membrane-mediated interaction, due to the overlap of such perturbations, is expected to be negligible for not too small distances between the contact lines.

(ii) The liquid phases outside and inside the vesicle and between the two lamellae are identical, that is, water. (If one of these phases were of different viscosity, which is not the case, one could expect significant deviations from the Stimson−Jeffrey formula, eq 3.3.)

(iii) Since the lipid lamellae are impermeable for water, the normal projection of the hydrodynamic velocity should be zero at the membranes. If the lipid lamellae are nearly tangential to the streamlines in the Stimson−Jeffrey problem, then eq 3.3 will give a satisfactory approximation for our system.

The fulfillment of the above three expectations seems to be confirmed by the good agreement between the experimental and computed particle trajectories, see section 5.1 below.

3.2. Meniscus Profile. The goal of this paragraph is to extract basic characteristics of the menisci shown in Figures 6 and 7. Essentially, we will treat the couple of particles in contact as a single particle and find tentative values of the parameters defined in Figure 2. These will be later injected as the constants entering the boundary conditions in the exact theory (section 4).

The single-particle approximation makes the system axisymmetric. In (r,z) coordinates (see Figure 2), the Laplace equation for the meniscus shape[2,32] reads

$$\frac{1}{r}\frac{d}{dr}(r\sin\psi) = \frac{P_c}{\sigma} \qquad \frac{dz}{dr} = \tan\psi \quad (3.7)$$

Here, ψ is the running slope angle. The ratio P_c/σ, whose value is not known a priori, can be determined by fitting eq 3.7 to the experimental profiles. These profiles are shown in Figures 6 and 7 (the graphs contain the points from both left- and right-hand side portions of the menisci). The solid lines in Figures 6b and 7b are the result of the fitting procedure. They can be extrapolated to find the

(44) Danov, K. D.; Dimova, R. I.; Pouligny, B. *Phys. Fluids* **2000**, *12*, 2711.
(45) Stimson, N.; Jeffrey, G. *Proc. R. Soc. London* **1926**, *A111*, 110.
(46) Taylor, P. *Proc. R. Soc. London* **1924**, *A108*, 11.
(47) Stone, H. A.; Ajdari, A. *J. Fluid Mech.* **1998**, *369*, 151.

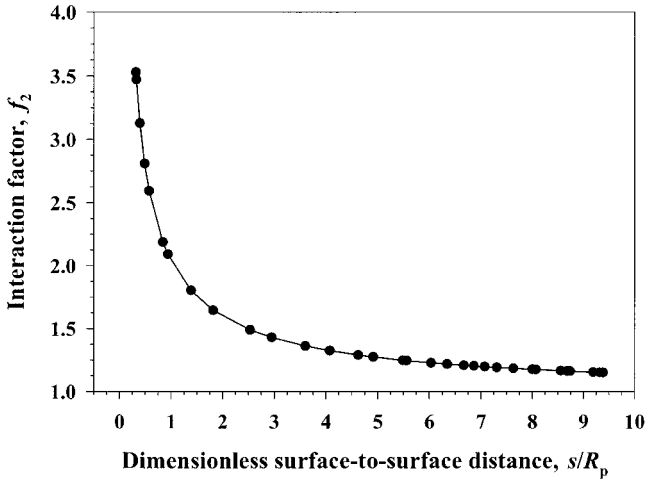

Figure 5. Hydrodynamic interaction factor, f_2, calculated by means of eq 3.3, as a function of the surface-to-surface distance between two particles, s, scaled with the particle radius, R_p.

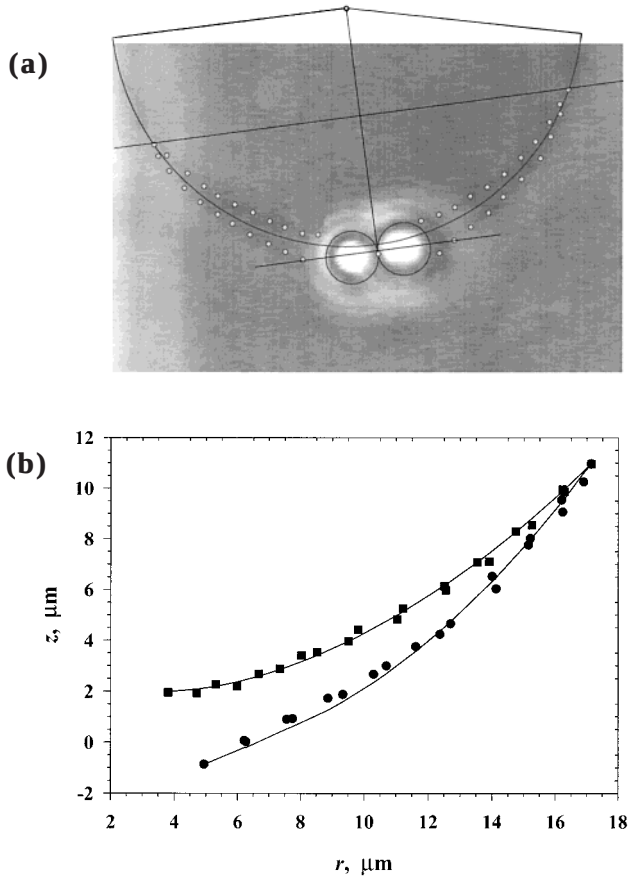

Figure 6. (a) Determining the positions of particles and menisci in Figure 3a by means of image analysis. (b) Processing of the data for the meniscus shape by means of the Laplace equation. Diameters of the vesicle and particles: $2R_v = 39\ \mu$m and $2R_p = 4.3\ \mu$m.

positions of the membrane−particle contact lines and that of the peripheral line.

As Figures 6 and 7 are perpendicular cross sections of the real, nonaxisymmetric system, one might expect that they give different values of the above parameters. In fact they do, but the differences are small. For instance, the values of the membrane−membrane contact angle, 2α, are 8.3° and 8.5°, and those of the encapsulated volume, V, are 1005 and 904 μm^3, respectively. In conclusion, the single-particle approximation yields coherent values. The

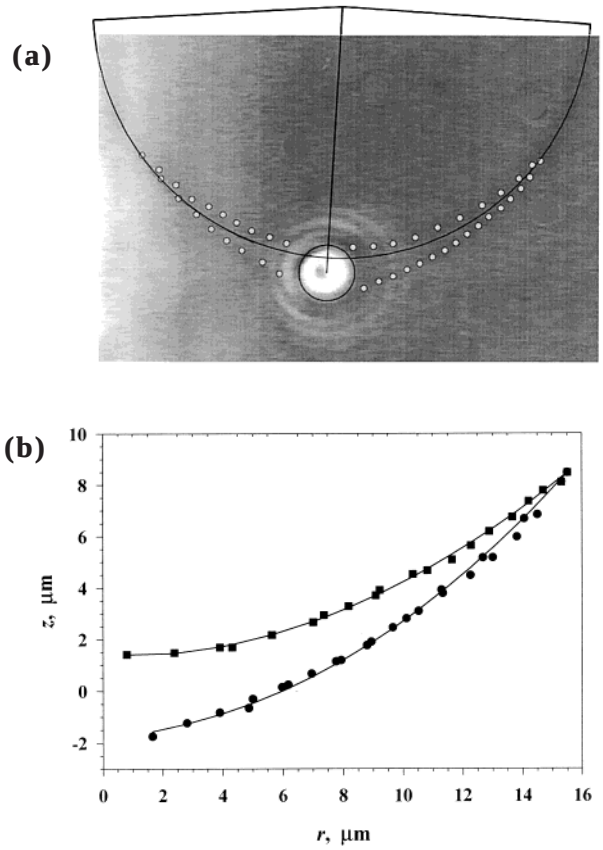

Figure 7. (a) Determining the positions of particles and menisci in Figure 3b by means of image analysis. (b) Processing of the data for the meniscus shape by means of the Laplace equation. Diameters of the vesicle and particles: $2R_v = 39\ \mu$m and $2R_p = 4.3\ \mu$m.

mean values, deduced from both figures, are $2\alpha \approx 8.4°$, $2h_c \approx 3.6\ \mu$m, and $V \approx 955\ \mu$m^3.

4. Theory and Computation Procedure

We now come to the theory of the lateral capillary force. In this section, we first calculate the shapes of menisci around the particles, which are now distinct and separated by a finite distance. From these shapes, we will deduce the capillary force and the interaction energy between the particles.

4.1. Computation of the Two-Particle Meniscus Shape. To find the meniscus shape, one has to solve the Laplace equation of capillarity, eq 1.1, using appropriate boundary conditions. In general, one could have the following types of boundary conditions: at the *particle surface*, (1) fixed contact line or (2) fixed contact angle; at the *meniscus periphery*, (A) fixed contact line or (B) fixed contact angle. Then, four combinations of boundary conditions, viz., 1A, 1B, 2A, and 2B, are possible. The solution of the resulting mathematical problem requires time-consuming computations. To simplify the problem, we used the following two approximations:

(i) We supposed a *planar* geometry, as in Figure 2;

(ii) We used the linearized Laplace equation, eq 1.6, instead of the nonlinear eq 1.1. For meniscus slopes smaller than 20°, we found numerically that the results from the linearized and nonlinear equations were very close to each other.

The symmetry of the system suggests using bipolar coordinates, see for example ref 33. These coordinates, denoted τ and ω, are defined through the following set of equations:

$$x = \chi \sinh \tau \qquad y = \chi \sin \omega \qquad \chi = a/(\cosh \tau - \cos \omega) \tag{4.1}$$

$$\frac{\partial^2 \zeta}{\partial \tau^2} + \frac{\partial^2 \zeta}{\partial \omega^2} = \chi^2 \frac{P_c}{\sigma} \tag{4.2}$$

As illustrated in Figure 8, the lines τ = const and ω = const are two families of mutually orthogonal circumferences. In eq 4.1, a is a parameter related to the radius of the contact line, $r_c = (R_p^2 - h_c^2)^{1/2}$, and to the distance between the two particles, L (see the triangle OAC in Figure 8):

$$a = [(L/2)^2 - r_c^2]^{1/2} \tag{4.3}$$

The use of bipolar coordinates greatly simplifies the solution of the boundary problem because the projections of the membrane−particle contact lines on the xy-plane are simply represented by $\tau = \pm\tau_c$, with $\tau_c = \text{arc cosh}[L/(2r_c)]$. Besides, because of the symmetry of the meniscus, the integration domain for eq 4.2 is contained in the ($0 \le \tau \le \tau_c$, $0 \le \omega \le \pi$) rectangle, see Figure 9.

To find the value of P_c/σ, we supposed that the total volume of the water in the Plateau border was constant, that is, independent of the particle-to-particle distance L:

$$V = 4 \int \int \zeta(\tau,\omega)\, \chi^2 \, d\tau \, d\omega = \text{const} \tag{4.4}$$

This amounts to assuming that the lipid bilayers are impermeable to water and that there is no encapsulated water beyond the peripheral line. In fact, the high value of the peripheral angle, $2\alpha = 8.4°$, implies that far from the particles the two bilayers adhere to each other. Hence, there is virtually no free water sandwiched between them.

We solved eq 4.2 by numerical integration, following the procedure described in Appendix B. We carried out preliminary computations with the four possible combinations of boundary conditions (see above) and with the values of V, α, and h_c determined in section 3.2. The tests lead us to selecting condition 1B (fixed contact line at the particle surface and fixed contact angle at the meniscus periphery), because it was the only one leading to a particle trajectory which was similar to the experimental one (Figure 4a).

4.2. Calculation of the Capillary Force. In general, the capillary force **F** exerted on each particle is a sum of contributions due to the pressure, integrated over the particle surface, and to the surface (membrane) tension, integrated along the contact line (for details, see refs 1, 2, and 11). Due to the symmetry of the system, **F** is directed along the x-axis, passing through the centers of the two particles. According to condition 1B, we deal with a horizontal and immobile contact line at the particle surface. For that reason, only the integral of the membrane tension contributes to the capillary force (the integral of pressure being zero):[1,2,11]

$$F_c = 2\mathbf{e}_x \cdot \oint_C d\mathit{l}\, \mathbf{m}\sigma \tag{4.5}$$

Here, F_c is the magnitude of the capillary force, $d\mathit{l}$ denotes a linear element along the contact line C on the particle surface, and $\mathbf{e}_x$ is the unit vector of the x-axis; **m** is a unit vector having the direction of the membrane-tension vector at the contact line; in other words, **m** is simultaneously tangent to the meniscus surface and perpendicular to C. The multiplier 2 in eq 4.5 accounts for the presence of two contact lines at the surface of each particle (Figure 2). To compute the integral, we defined a polar coordinate system

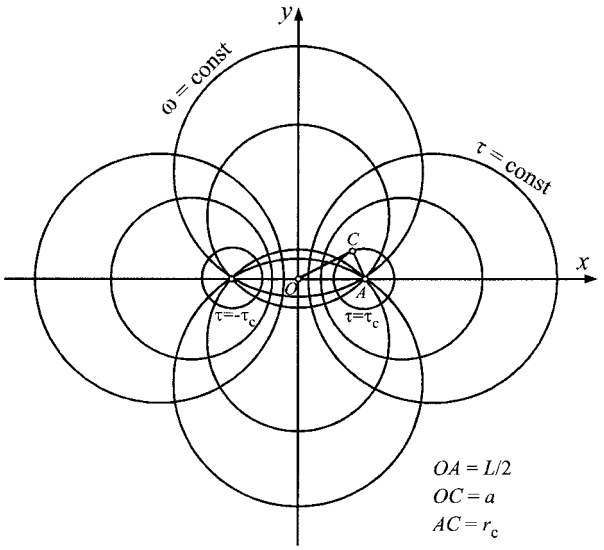

Figure 8. Bipolar coordinates (τ,ω) in the xy-plane. The τ = const and ω = const coordinate lines represent two families of mutually orthogonal circumferences. The contact lines on the particle surfaces correspond to $\tau = \pm\tau_c$. Point A denotes the center of the circumference $\tau = \tau_c$; A is close to (but not identical with) the right-hand side pole of the bipolar coordinates.

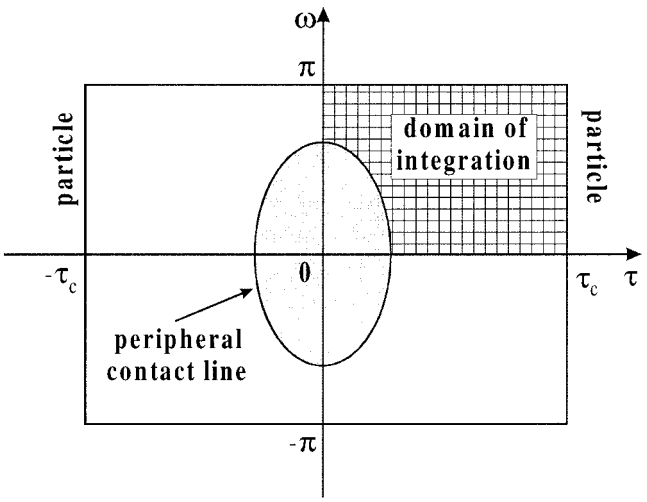

Figure 9. Sketch of the integration domain for the Laplace equation, eq 4.2. Due to the symmetry of the system, the integration is carried out in the first quadrant; the corresponding area is denoted by a grid-hatching. The bipolar coordinates transform the peripheral contact line of the Plateau border into an oval; its interior (shadowed) corresponds to the zone outside the overlapping menisci, where $\zeta = 0$; the coordinate origin in the $\tau\omega$-plane is the infinite point in the xy-plane.

(r,φ) whose origin is taken at the center of the contact line of one of the two particles. Then, we have

$$d\mathit{l} = r_c d\varphi \qquad \mathbf{m} = \mathbf{e}_r \cos \psi_c - \mathbf{e}_z \sin \psi_c \tag{4.6}$$

where $\mathbf{e}_r = \mathbf{e}_x \cos \varphi + \mathbf{e}_y \sin \varphi$ is the unit vector in the radial direction and ψ_c is the meniscus slope angle at the contact line:

$$\tan \psi_c = -\frac{\partial \zeta}{\partial r}\Big|_{r=r_c} = \frac{1}{\chi}\frac{\partial \zeta}{\partial \tau}\Big|_{\tau=\tau_c} \tag{4.7}$$

Further, in view of eqs 4.6 and 4.7, one obtains

$$\mathbf{e}_x \cdot \mathbf{m} = \cos \psi_c \cos \varphi \approx \left[1 - \frac{1}{2}\left(\frac{1}{\chi}\frac{\partial \zeta}{\partial \tau}\right)^2_{\tau=\tau_c}\right] \cos \varphi \tag{4.8}$$

Finally, substituting eqs 4.6 and 4.8 into eq 4.5 gives

$$F_c = 2\sigma r_c \int_0^{\pi} d\varphi \cos\varphi \left(\frac{1}{\chi}\frac{\partial\zeta}{\partial\tau}\right)^2_{\tau=\tau_c} \quad (4.9)$$

Due to the symmetry of the system, the integration domain is taken to be half of the contact line, $0 \le \varphi \le \pi$; correspondingly, a multiplier 2 is added in eq 4.9. At the contact line, the bipolar coordinate ω is related to the azimuthal angle φ as follows:[2,48]

$$\cos\omega = \frac{(L/2)\cos\varphi + r_c}{r_c \cos\varphi + L/2} \qquad (\tau = \tau_c;\ 0 \le \varphi \le \pi) \quad (4.10)$$

To calculate the integrand in eq 4.9 for a given φ, we determine ω from eq 4.10 and then we calculate $\partial\zeta/\partial\tau$ from the numerical solution $\zeta(\tau,\omega)$ of eq 4.2 for $\tau = \tau_c$. Afterward, the value of F_c is found by numerical integration in eq 4.9; see Appendix B for details.

4.3. Calculation of the Interaction Energy. The capillary interaction energy, ΔW, can be calculated by integration of the force profile. An equivalent but more direct and accurate method is to calculate ΔW from the meniscus shape. The procedure is as follows: we start with the grand thermodynamic potential for the two-particle system,

$$\Omega = -P_c V + 2\sigma A_m + \gamma(A_{tot} - A_p) \quad (4.11)$$

$2A_m$ is the total meniscus area (incl. the upper and lower menisci). A_p is the area of the meniscus projection on the xy-plane; A_{tot} is the total membrane area, which is assumed finite and constant; $\gamma = 2\sigma\cos\alpha$ is the tension of the bilamellar membrane. Equation 4.11 is general. The potential for noninteracting particles (such as in Figure 2) reads

$$\Omega^{(0)} = -P_c^{(0)} V + 2\sigma A_m^{(0)} + \gamma(A_{tot} - A_p^{(0)}) \quad (4.12)$$

where the (0) superscript refers to the case of nonoverlapping menisci. The capillary interaction energy is then

$$\Delta W \equiv \Omega - \Omega^{(0)} = -(P_c - P_c^{(0)})V + 2\sigma[(A_m - A_m^{(0)}) - (A_p - A_p^{(0)})\cos\alpha] \quad (4.13)$$

The meniscus area is related to the meniscus shape, $z = \zeta(\tau,\omega)$, through the expression

$$A_m = 4\int_0^{\tau_c}\int_0^{\pi} (1 + |\nabla_{II}\zeta|^2)^{1/2} M(\tau,\omega)\,\chi^2\, d\tau\, d\omega \quad (4.14)$$

where ∇_{II} and χ are defined by eqs 1.2 and 4.1. $M(\tau,\omega)$ is an auxiliary function: $M = 1$ for a point inside the domain of integration (see Figure 9), and $M = 0$ otherwise. Likewise, A_p is given by eq 4.14 with $\zeta \equiv 0$.

Recall that the meniscus shape and the P_c/σ ratio are fixed by the V = constant condition (eq 4.4). So are the surface areas, A_m and A_p. Consequently, for a given L, the value of V determines that of the $\Delta W/\sigma$ ratio.

5. Numerical Results and Discussion

5.1. Comparison of Theory and Experiment. Line characteristics (see Figure 2), such as the radii of the membrane−particle contact line and of the peripheral line around a separate particle, can be deduced as described in section 3.2; in particular, $r_c = 1.2\,\mu$m, and $r_p = 13.7\,\mu$m. Having computed the capillary and drag forces, $F_c(s,\sigma)$ and $F_d(s)$, and substituting them into eq 3.1, one can calculate the theoretical trajectory, $\theta(t)$, and compare it to the experimental one; see Figure 4a and the computational procedure in Appendix B. In this procedure, the membrane tension σ is the only unknown parameter, to be determined from the best fit to the experimental curve. The result (solid line) is shown in Figure 4a. It was obtained with $\sigma = 6.4 \times 10^{-3}$ mN/m. Note that such a small tension is typical for flaccid lipid membranes.[49] From the values of α and σ, one can compute the *energy of adhesion* per unit area of the two lipid bilayers of our bilamellar membrane: $w_a = 2\sigma(1 - \cos\alpha) = 3.4 \times 10^{-5}$ erg/cm^2. The latter value corresponds to a "weak" adhesion in the classification of Evans.[49]

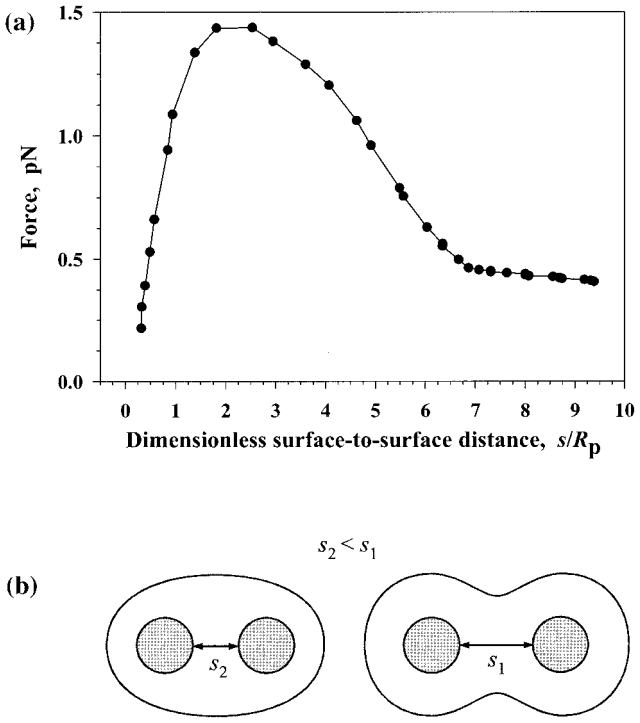

Figure 10. (a) Force vs distance dependence, F_c vs s/R_p, determined from the best fit of the data in Figure 4a applying the procedure described in Appendix B. (b) For the larger distances, the shape of the peripheral line has two symmetric concavities, which disappear for short distances; the maximum value of F_c roughly corresponds to the distance at which the two concavities disappear.

The data of Figure 4a are shown in Figure 4b in a velocity-versus-distance representation, $v = v(s)$. The velocity is almost constant for large s and increases up to a maximum at a small but finite distance ($s^* \approx 5\,\mu$m). The capillary force profile, our central result, is shown in Figure 10a. Note that the $v(s)$ and $F_c(s)$ profiles are similar but not exactly proportional, because of the hydrodynamic interaction between the particles when they come close to contact (see section 3.1). F_c is found to be $\approx$1 pN for $s \approx 2\,\mu$m, in accordance with the *independent* estimate from the maximum force of the optical trap (see section 2.3).

We find that for large s, the peripheral line has two symmetric concavities at mid-distance between the two particles. When s is decreased, these concavities disappear and the peripheral line becomes completely convex. The maximum of the capillary force (Figure 10a) roughly corresponds to the distance at which the two concavities disappear (Figure 10b).

(48) Paunov, V. N.; Kralchevsky, P. A.; Denkov, N. D.; Ivanov, I. B.; Nagayama, K. *Colloids Surf.* **1992**, *67*, 119.
(49) Evans, E. *Adv. Colloid Interface Sci.* **1992**, *39*, 103.

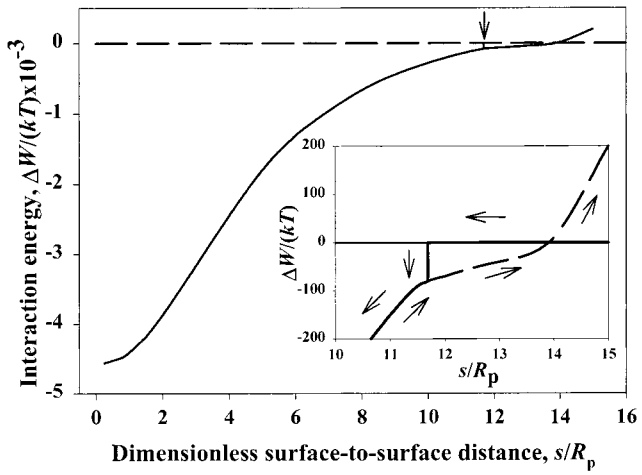

Figure 11. Plot of the capillary interaction energy, ΔW, vs s/R_p, calculated from eq 4.13; all parameter values are the same as in Figure 10. The arrows in the inset show that the ΔW vs s/R_p dependence is different on approach and separation. On approach, ΔW exhibits a jump at a distance, corresponding to the first contact of the peripheral lines of the two (initially separate) Plateau borders.

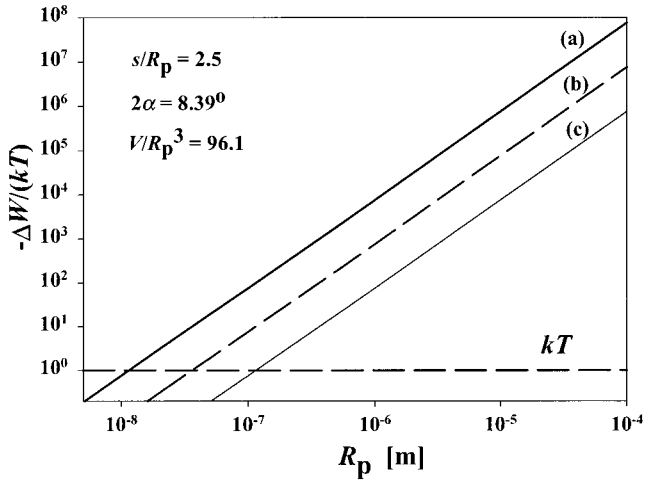

Figure 12. Plot of the capillary interaction energy, ΔW, vs particle radius, R_p, for a fixed dimensionless surface-to-surface separation, $s/R_p = 2.5$, and for three values of the meniscus tension: (a) $\sigma = 0.064$ mN/m, (b) $\sigma = 0.0064$ mN/m, and (c) $\sigma = 0.00064$ mN/m. The variation of R_p at fixed σ corresponds to the consideration of geometrically similar particle/menisci configurations of variable size (scaled with R_p), but with the same interfacial tension.

5.2. Energy Profile and Hysteresis. Figure 11 shows the interaction energy, ΔW, calculated by means of eq 4.13 using the same conditions and parameter values as for the force-versus-distance curve, $F_c(L)$ (by numerical differentiation, we checked that the derivative of the energy, $d(\Delta W)/dL$, coincides with the force calculated from eq 4.9). The energy unit in Figure 11 is kT, the thermal energy. Notice that for $s < 6R_p$ we have $|\Delta W| > 1000\ kT$, which means that the capillary attraction completely overwhelms the Brownian motion of the particles and leads to their irreversible aggregation.

When the particles are separated by a very large distance, their menisci do not overlap and there is basically no interaction: $\Delta W = 0$. When the separation is decreased, the system follows the $\Delta W = 0$ line down to the point marked by a vertical arrow in Figure 11. This is the point where the initially separated peripheral lines touch each other (this corresponds to $L = 2r_p$ in Figure 2). At this distance, the Plateau borders around the two particles merge and form a united Plateau border. Note that the shape of the united meniscus is not a superposition of the initially separate menisci. Indeed, the shape of the peripheral contact line of the united Plateau border cannot be found by a mere overlap of the two circular peripheral lines of the respective particles in isolation. This abrupt change in the meniscus shape induces a corresponding jump in ΔW, which is about 100 kT for the considered specific system.

In contrast, if we start from the aggregated particles state ($s = 0$) and increase s, ΔW gradually increases without any jump at $L = 2r_p$ (inset in Figure 11, the lower arrows). Upon a further increase of the interparticle distance, ΔW becomes positive, which means that the energy corresponding to a state with one united meniscus is greater than the energy of the state with two separate menisci. In other words, the splitting of the united meniscus to two separate menisci becomes energetically favorable. We thus find that the connexity transition, between the two-separate-menisci and the one-meniscus states, is discontinuous and leads to hysteresis. As a consequence, the capillary interaction energy cannot be computed starting from the separate-menisci state and applying a superposition approximation. Note that we have identified transition points, not stability limits. The latter can be found only from a stability analysis, which we did not work out yet.

This hysteresis phenomenon has a "three-dimensional" analogue: when particles covered by liquid films approach each other, they jump into strong adhesion contact; however, their separation requires pulling them much further than the original point of contact due to the extension of the liquid bridge between them.[50,51] Similar hysteresis of the force behavior has been detected by atomic force microscopy (AFM) when a solid colloidal particle interacts with a gas bubble or a liquid drop.[52−54]

5.3. Dependence of ΔW on Particle Size. The analysis of the equations (section 4) shows that ΔW can be expressed in the following scaled form:

$$\frac{\Delta W}{\sigma R_p^2} = f\left(\frac{L}{R_p}, \frac{r_c}{R_p}, \frac{V}{R_p^3}, \alpha\right) \qquad (5.1)$$

where f is a universal function. We computed ΔW for different particle sizes, with the same ratios of the geometrical parameters as in the experimental system, viz., $r_c/R_p = 0.547$, $V/R_p^3 = 96.1$, and $2\alpha = 8.39°$, and for a dimensionless distance between the two particles: $s/R_p = 2.5$ (that is, $L/R_p = 4.5$). In other words, we compared systems that differ only by a dilatation factor, that is, up- or downscaled versions of the experimental system. This choice makes the right-hand side of eq 5.1 constant, and we simply have $\Delta W \propto \sigma R_p^2$. Results are shown in Figure 12, for three different values of the film tension, in log−log representation. Line b corresponds to the experimental tension, $\sigma = 0.0064$ mN/m, and the other two lines correspond to 10 times larger or smaller σ. Clearly, the capillary attraction energy for micrometer-sized particles is everywhere considerably larger than kT. It becomes on the order of kT only for very small particles, namely, for R_p between 10 and 100 nm. It is amazing that even at

(50) Pitois, O.; Moucheront, P.; Chateau, X. *J. Colloid Interface Sci.* **2000**, *231*, 26.
(51) Feng, C. L.; Yu, A. B. *J. Colloid Interface Sci.* **2000**, *231*, 136.
(52) Preuss, M.; Butt, H.-J. *J. Colloid Interface Sci.* **1998**, *208*, 468.
(53) Preuss, M.; Butt, H.-J. *Langmuir* **1998**, *14*, 3164.
(54) Ecke, S.; Preuss, M.; Butt, H.-J. *J. Adhes. Sci. Technol.* **1999**, *13*, 1181.

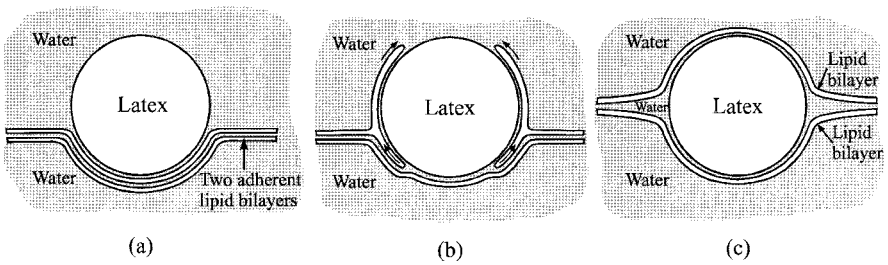

Figure 13. Three consecutive stages of the entrapment of a latex sphere into the membrane of a bilamellar lipid vesicle: (a) The latex particle just after its contact with the membrane. (b) The upper lipid lamella spreads over the upper bare surface of the particle and "dewets" its lower surface, driven by the energy gain accompanying the lipid-to-latex adhesion. (c) At the final stage, the latex sphere, together with some permeate of water, is encapsulated between the two lipid bilayers.

such low interfacial (membrane) tensions the capillary force can bring about considerable attraction between submicrometer particles.

6. Summary and Conclusions

In this study, we considered particles which are confined in a liquid film or bilamellar lipid vesicle. The system can be viewed as a pair of interfaces (the two adsorption monolayers that compose a soap film or the two bilayers of a bilamellar lipid vesicle), which are everywhere in adhesive contact in the nonperturbed state. Between the two film surfaces, one or two colloidal particles have been inserted, which are considerably larger than the nonperturbed film thickness (Figure 2). Each particle creates a meniscus, that is, a region where the films are separated, and whose inside is filled with water. We argued that this type of meniscus is *finite*, that is, bounded by a *peripheral line* at a finite distance from the particles. This is in contrast with, for instance, capillary depressions caused by gravity around massive particles at the water/air interface. As is well-known, the latter type of meniscus is infinite, as it decays exponentially at infinity. From the mathematical viewpoint, the cases of finite and infinite menisci are different, as they correspond to different forms of the Laplace equation of capillarity, cf. eqs 1.3 and 1.6.

We studied the capillary interaction between finite menisci, experimentally and theoretically. Experiments with particles encapsulated between the membranes of a bilamellar giant lipid vesicle clearly revealed the interaction, which showed up as an attraction between the particles. From the particle trajectories and by optical dynamometry, we observed that the attraction force was long-ranged (several micrometers) and that it would reach a maximum, on the order of a piconewton, when the particles were separated by a distance comparable to their radius.

To interpret the experimental findings, we determined the shape of the menisci by solving the Laplace equation (eq 4.2) in bipolar coordinates and deduced the capillary force between the particles as a function of their separation. The calculated force was used to interpret the experimental particle trajectory (Figure 4a), from which we deduced the values of the film tension, σ, and adhesion energy, w_a. The fact that the experimental trajectory was excellently fitted to by variation of a single adjustable parameter, σ, indicates that the theoretical model is adequate. In addition, the magnitude of the determined capillary force agrees well with the independent estimate obtained by optical dynamometry.

At this point, it is worth emphasizing that the nonmonotonic variation of the capillary force versus the interparticle distance (Figure 10) is characteristic of the finite-meniscus problem (infinite menisci would produce a monotonic variation). A second characteristic is the discontinuous transition between the configurations of separated and fused menisci. The discontinuity should show up as *hysteresis* in the force profile, according to whether the interparticle distance is increased (from zero) or decreased (from large separation, where the particles do not interact), see Figure 11. At this stage, the hysteresis is a theoretical prediction, which has not been experimentally proven yet, and could be the matter of future experiments.

We found that ΔW, the capillary attraction energy of the micrometer-sized particles in the investigated experimental system, was considerable, on the order of 1000 kT at contact. Thus, the interaction drives an irreversible aggregation of the particles. If the system is simply up- or downscaled, ΔW is predicted to vary as σR_p^2. Even with the very low tensions of flaccid vesicle membranes ($\sigma =$ 0.064 mN/m in our example), ΔW is still on the order of kT for particles of radius $\approx$10 nm, see Figure 12. Consequently, the capillary immersion force can be important down to nanometric particle sizes and cause aggregation and ordering of the particles.

Acknowledgment. This study was carried out in the framework of the Franco-Bulgarian Laboratory "Vesicles and Membranes" supported by CNRS, France. We are indebted to G. Gréhan and G. Gouesbet for the kind provision of the GLMT program used to compute the radiation pressure forces, and we gratefully acknowledge the participation of M. I. Angelova in some of the described experiments.

Appendix A: Discussion on the Mechanism of Encapsulation

The initial stage of attachment of a latex sphere to a bilamellar membrane is depicted in Figure 13a, whereas the final state is sketched in Figure 13c; cf. the photographs in Figure 3. The transition from the initial to the final state occurs very quickly, and it cannot be resolved by the available video technique. The intermediate stage, between those in parts a and c of Figure 13, is not known. A tentative scenario, which upgrades the model suggested in ref 40, is sketched in Figure 13b. The strong adhesion of the lipid to the latex particle makes favorable the spreading of the upper lipid bilayer over the surface of the adhering particle. However, such a bilayer cannot survive a direct molecular stretch larger than 5−10%, see for example ref 49. For that reason, it might energetically favorable for the upper bilayer to break below the latex particle and to completely cover the bare upper portion of the latex particle (Figure 13b). Before closing of the spreading bilayer at the "north pole" of the latex particle, some water could penetrate between the bilayer and the particle and remain captured between the two lipid

lamellae to form the Plateau border, see Figure 13c. The process depicted in the latter figure should happen spontaneously insofar as it is accompanied with a decrease in the free energy of the system owing to the gain of adhesion energy between the lipid membrane and the latex particle surface.

Appendix B: Principles of the Numerical Procedure

1. The input parameters are the volume V of the water enclosed in the Plateau borders and the geometrical parameters L, h_c, r_c, α, and r_p; see Figure 2 for the notation.

2. To initiate the computation, we first approximate the shape of the peripheral contact line by two overlapping circumferences of radius r_p.

3. Next, we assume a zeroth-order approximation for the unknown parameter $p = p^{(0)} \equiv P_c/\sigma$. We take that obtained from the analysis of Figure 6 or Figure 7 by the axisymmetric approximation (see section 3.2).

4. Imposing $\zeta = h_c$ at the particle contact line and $\zeta = 0$ at the peripheral line of the Plateau border as boundary conditions, we numerically integrate the linearized Laplace equation, eq 4.2. Bipolar coordinates (τ,ω) are used, see eq 4.1 and Figure 8. Because of the symmetry of the system, it is sufficient to carry out the integration in a $^1/_4$ part of the meniscus projection on the horizontal plane. The domain of integration (Figure 9) is discretized through a 100×100 grid. We apply a second-order numerical method (with respect to the computational time), namely, the Alternating Direction Implicit method.[55]

5. After solving eq 4.2 and determining $\zeta(\tau,\omega)$, we compute the value of the volume $V^{(k)}$ ($k = 0,1,2,...$) corresponding to the input value, $p^{(k)}$, of the parameter p; in general, $V^{(k)} \neq V$.

6. We repeat steps 4 and 5 for $p^{(k+1)} = p^{(k)} + \Delta p$, where Δp is a small variation, and we compute $V^{(k+1)} = V^{(k)} + \Delta V$. As the next approximation, we take $p = p^{(k+2)} = p^{(k)} + (\Delta p/\Delta V)(V^{(k)} - V)$ and repeat steps 4−6. Typically, 7−10 cycles are sufficient to achieve $(V^{(k)} - V)/V \leq 10^{-5}$. Thus, we determine the value of p which corresponds to the input value of V.

7. In general, the meniscus shape $\zeta(\tau,\omega)$ computed in this way does not obey the boundary condition $\partial\zeta/\partial n = \tan\alpha = \text{const}$ at the peripheral contact line. To satisfy the latter condition, we change the shape of the peripheral contact line as follows. Where the peripheral contact angle is greater than α, we expand the contact line by one grid-node in the normal direction; where the contact angle is less than α, we shrink the contact line by one node in the normal direction; where the contact angle is equal to α, we do not vary the position of the peripheral contact line (see Figure 9). Then, we repeat steps 4−6 and determine new values of p and $\zeta(\tau,\omega)$.

8. If the peripheral contact angle is not everywhere equal to α (within a prescribed accuracy), step 7 is repeated. Typically, from 20 up to 40 iterations are needed; their number increases when the interparticle distance L decreases. Ultimately, we obtain the values of p and $\zeta(\tau,\omega)$ which satisfy all boundary conditions.

9. With the obtained $\zeta(\tau,\omega)$, we compute the capillary force F_c from eq 4.9 using a tentative value of the unknown membrane tension σ.

10. Finally, we numerically solve eq 3.1 along with the eqs 3.2−3.6 for the drag force F_d; thus, we determine the theoretical trajectory of the particle, $\theta(t)$. The adjustable parameter σ is varied until the best fit of the experimental data for $\theta(t)$ is achieved, see Figure 4a. With the value of σ thus determined, we compute the adhesion energy per unit area of the lipid bilayers, $w_a = 2\sigma(1 - \cos\alpha)$.

LA0107300

(55) Fletcher, C. A. J. *Computational Techniques for Fluid Dynamics*; Springer: New York, 1991; Vols. I and II.